Research Article

Maxwell Fluid Performance on Free Convective Non-Newtonian Nanofluid Flow Over a Cone in Presence of Magnetic Field, Heat and Mass Transfer

M. Sathyanarayana*[1] [iD] and T. Ramakrishna Goud[2] [iD]

[1] *Department of Mathematics, University College of Science, Osmania University, Hyderabad 500007, Telangana, India*
[2] *Department of Mathematics, University College of Science, Saifabad, Hyderabad 500004, Telangana, India*
*Corresponding author: manthrisathyam926@gmail.com

Abstract. In this research work, the numerical technique called Runge-Kutta method along with shooting technique is used to find the numerical solutions in the presence of magnetic field, heat and mass transfer on steady, two-dimensional, viscous, incompressible, electrically conducting, Maxwell fluid flow towards a vertical cone with the effects of Thermophoresis and Brownian motion effects. For this investigation, the basic governing equations for this fluid flow were transformed into non-linear ODEs using the similarity quantities. Graphical visualizations of velocity, temperature, and concentration distributions are shown with the effects of various engineering parameters. Also, the numerical values of engineering quantities Skin-friction, Nusselt number and Sherwood number coefficients are presented in tabular forms. Finally, for program code validation, the present numerical results are compared with the published results available in literature. In this current work, the velocity profiles are decreasing with increasing values of Maxwell fluid and Magnetic field parameters. With the increasing effects of Brownian motion and thermophoresis the temperature profiles are increase. The concentration profiles are increasing with increasing values of thermophoresis parameter and reverse effect is observed in case of Brownian motion effect. Also, the concentration profiles are decreasing with rising values of Lewis number.

Keywords. Maxwell fluid, Nanofluid, Free convection, Magnetic field, Heat transfer, Mass transfer

Mathematics Subject Classification (2020). 76W05, 76R50, 76D05, 76A05

1. Introduction

Industrial, scientific, and engineering applications have been crucial in the development of feasible systems for the transfer besides non-Newtonian liquids of mass then heat. Fluids that are not Newtonian are known as non-Newtonian fluids. That just do not behave according to Nutrition, lotions, droplets, heavy oils, and blood, cosmetics, toothpaste, and waste fluids are non-Newtonian liquid instances. Slurries and gels remain further examples. Non-Newtonian fluid flows have heat and mass transport characteristics that vary significantly from Newtonian fluids. The formulas which control non-Newtonian liquid have non-Newtonian stream. Substantially more complicated and extensively connected to other nonlinear equations than the Newtonian fluid stream ruling formulas. Because of the considerable nonlinearity involved, obtaining enclosed type of a solution aimed at a liquid that is not Newtonian flow stays almost impossible. The Maxwell liquid formed when the characteristics of elasticity and viscosity of a substance are combined (Christensen [3]). This idea was proposed in 1867 besides James Clerk Maxwell. The liquid model can make predictions regarding the consequences of relaxation time. Fluids of the differential kind are incapable of predicting such effects. Because of its capacity to anticipate the behaviour of low-molecular-weight polymers, this fluid model is very valuable for analysing them. A Maxwell fluid is the rate type, and Maxwell fluids include lubricants, crude oil, and polymer solutions. Zhao *et al*. [27] examined unstable unsurprisingly occurring Flow field Maxwell on vertical flat apparent using frontier sheet approximations. Ramesh and Gireesha [20] investigated effects about a origin of hot air or on either a Maxwell fluid faucet on stretched as for surface a pattern develops for convection using nanoparticles. They conducted their study in the presence of nanoparticles. Madhu *et al*. [15] discovered unstable to radioactivity, getting stretched sheet stream of Maxwell fluid and nanoparticles influence in their research. They observed that when the unsteadiness term was raised, the skin friction coefficient reduced, which was owing to the radiation effect causing the nanoparticles to move faster. Mukhopadhyay [16] calculated how heat would transfer across a stretched sheet in a Maxwell liquid that is temporary either a supplier of heat or a heat descends. Khan *et al*. [13] investigated the divisions and thermophoretic effects happening Maxwell fluid MHD stream towards stretched surface. Zhao *et al*. [26] Dufour but also Soret were explored, effects utilising permeable exteriors MHD Fluid Maxwell. In addition to Dumitru and Abdul [7] studied movement out of partition while Stokes flows were operating on a Maxwell fluid in a slip situation. Ramesh *et al*. [21] proposed a three-dimensional Maxwell fluid that approaches a stretched surface through heat radiation and suspended nanoparticles. Sajid *et al*. [23] investigated the impact of potential energy and variation heat conduction transferred via stretched exterior on the Maxwell fluid. Zheng *et al*. [30] used an accelerating plate that oscillated and continued to move at a consistent pace to imitate the generalised Maxwell fluid. Ahmad *et al*. [1] investigated unstable Maxwell base fluid circulate in three-dimensions on a strained canvas. The flow's viscosity and thermal conductivity were changing. Chu *et al*. [5] studied thermophoretic particles deposition features in thermally developed flow of Maxwell

fluid between two infinite stretched disks. Khan *et al.* [14] designed modelling and found the dual solutions for magnetized mixed convective stagnation point flow of upper convicted Maxwell fluid model with second-order velocity slip. Khan *et al.* [12] developed a new idea of fractal-fractional derivative with power law kernel for free convection heat transfer in a channel flow between two static upright parallel plates.

Chu *et al.* [6] studied the characteristics of hybrid ferrofluid along with MWCNT for augmentation of thermal behaviour of fluid during natural convection in a cavity. Chu *et al.* [4] studied significance of activation energy, bio-convection and magnetohydrodynamic in flow of third grade fluid towards stretched surface using a Buongiorno model analysis. Zhao *et al.* [28] applied artificial neural networking analysis for heat and entropy generation in flow of non-Newtonian fluid between two rotating disks. Zhao *et al.* [29] studied entropy generation approach with heat and mass transfer in magnetohydrodynamic stagnation point flow of a tangent hyperbolic nanofluid. Sathyanarayana *et al.* [24] studied MHD nanofluid flow towards a vertical cone under convective cross-diffusion effects through numerical solutions. Song *et al.* [25] studied bio-convection analysis for sutter by nanofluid over an axially stretched cylinder with melting heat transfer and variable thermal features using a Marangoni and solutal model.

The investigation about mass and heat combined transmission as of various geometries is critical for a broad range of implementations in geophysics and technology. These applications include power transmission hydropower converter electronic parts reservoir formation, semi-conductor electronics heating and cooling, packed bed enzymatic power plants, insulation, and solar panels ([9] and [22]). Eid and Mabood [8] investigated temperature and mass in a viscoelastic fluid transfer through stretch a highly permeable channel with permeable surface using quantitative approaches. Nawaz *et al.* [18] used a theory that was not reliant on the Fourier transform to investigate the effect coefficient values on heat and mass that are dependent on temperature transit fluids that are deformable. Hamid *et al.* [10] investigated effects lipping through natural temperature but also mass advection transport in Liquid *Pr* quantity, but they did not include nanoparticles in their analysis. Hayat *et al.* [11] researched heat transmission during the stream of triplicate Prandtl liquid while it was heated by thermal radiation. Rajesh *et al.* [19] investigated heat and mass transport in a tapered radiation channel using a Prandtl liquid pulsatile stream in MHD. Mythreye *et al.* [17] used a vertically penetrable quasi moving plate with heat absorption to investigate impact about compound reactions scheduled unsteady MHD convective Thermal conduction and mass transfer.

The particular literature review cited above confirms that little attention is paid to the combine study of Maxwell and nanofluids for an incompressible, viscous, electrically conducting, viscous, magnetohydrodynamic flow past a vertical cone. This study is valuable because it has a wide range of applications in domains including medical sciences (treatment of cancer therapeutics), microelectronics, biomedicine, biology, and industrial production processes. Motivated by the above applications, the current study deals with the numerical analysis of non-Newtonian fluids subject to nanoparticles. Very recently, MHD Maxwell-nanofluid flow with

Runge-Kutta method along with shooting technique, off-late, to the best of authors knowledge a little attention is given for the Maxwell-nanofluid flow with heat and mass transfer. Therefore, the prime interest of the current investigation is to provide numerical solutions for a two-dimensional Maxwell (non-Newtonian) while in involvement of nanoparticles, heat and mass transfer along a vertical cone that is steady, electrically conductive, viscous, and incompressible. The study will concentrate on the influence of these variables. Similarity transformations for this issue are explored in this article, and the Runge-Kutta technique is utilised to do numerical analysis on equations that do not have dimensions. The continuity, momentum, energy, and concentration equations are employed in this study. The contribution of a large number of key features inherent in the flow system may be assessed using graphical representations. The publication's surviving segments are organised as: Section 2 consists of constructing the calculations that govern as well as similarity reduced versions of those equations. Section 3 employs the Runge-Kutta technique to get for just the calculations fields of air temperature, velocity and concentration. Section 4 provides a simple overview of the program's code validation. Section 5 contains the results and the author's comment. Some findings are reported in Section 6.

2. Flow Governing Equations

In this work, the results of buoyancy force, steady, two-dimensional, viscous, incompressible Maxwell-nano fluids move across a vertical a cone is studied. For this study the following assumptions are made:

  (i) Designed x-axis that also differs along the exterior of such cone, as well as the y-axis, and that is vertical, make up the coordinate's structure.

 (ii) The thermal boundary proportions can shift along the cone's exterior.

(iii) As seen in the Figure 1, a varying magnetic field B_o is implemented in the x-axis.

(iv) The implications of thermal convection were also taken into account, as well as a changeable temp.

 (v) The air temp but rather fluid intensity is T_∞ and C_∞.

(vi) The temperature difference and fluid density are represented by T and C, respectively.

(vii) Also, thermal diffusion, chemical reaction and diffusion thermos effects are overlooked.

Based mostly on foregoing inferences, following dimensional form of equations, under boundary-layer approximations governs the fluid stream of Maxwell-Nano fluid particles are

Equation of Continuity:

$$\frac{\partial(ru)}{\partial x} + \frac{\partial(rv)}{\partial y} = 0. \tag{2.1}$$

Equation of Momentum:

$$u\left(\frac{\partial u}{\partial x}\right) + v\left(\frac{\partial u}{\partial y}\right) + \gamma_1\left(u^2\frac{\partial^2 u}{\partial x^2} + v^2\frac{\partial^2 u}{\partial y^2} + 2xy\frac{\partial^2 u}{\partial x\partial y}\right)$$

$$= \nu_f\left(\frac{\partial^2 u}{\partial y^2}\right) - \left(\frac{\sigma B_o^2}{\rho_f}\right)u + \{(T - T_\infty) + (C - C_\infty)\}g(\rho\beta)_f\cos\alpha. \tag{2.2}$$

Equation about Thermal Energy:

$$u\left(\frac{\partial T}{\partial x}\right) + v\left(\frac{\partial T}{\partial y}\right) = \alpha^*\left(\frac{\partial^2 T}{\partial y^2}\right) + \tau\left\{D_B\left(\frac{\partial C}{\partial y}\right)\left(\frac{\partial T}{\partial y}\right) + \frac{D_T}{T_\infty}\left(\frac{\partial T}{\partial y}\right)^2\right\}. \tag{2.3}$$

Equation of species concentration:

$$u\left(\frac{\partial C}{\partial x}\right) + v\left(\frac{\partial C}{\partial y}\right) = D_B\left(\frac{\partial^2 C}{\partial y^2}\right) + \frac{D_T}{T_\infty}\left(\frac{\partial^2 T}{\partial y^2}\right), \tag{2.4}$$

and demarcation circumstances for this flow remain

$$\left.\begin{array}{l} u = 0,\ v = 0,\ T = T_w,\ C = C_w,\ \text{at } y = 0, \\ u \to 0,\ T \to T_\infty,\ C \to C_\infty,\ \text{as } y \to \infty. \end{array}\right\} \tag{2.5}$$
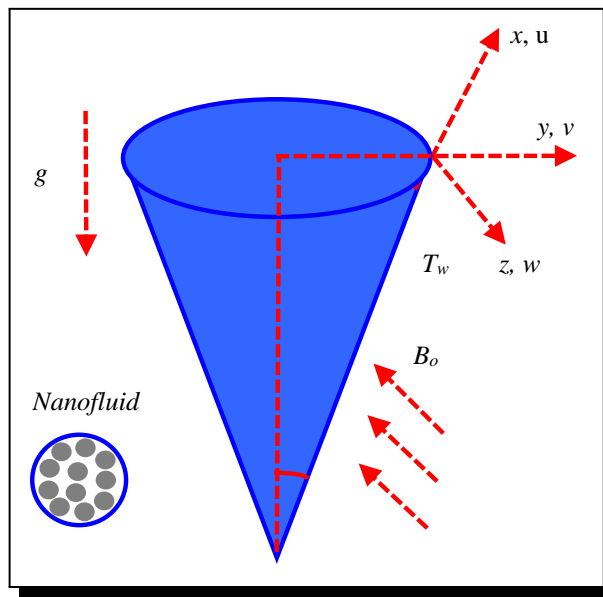

Figure 1. Physical scheme of framework and coordinates

Here the mechanism of stream is described for example

$$u = \frac{1}{r}\left(\frac{\partial \psi}{\partial y}\right).$$

Then

$$v = -\frac{1}{r}\left(\frac{\partial \psi}{\partial x}\right). \tag{2.6}$$

The continuity eq. (2.1) is identically satisfied. The following similarity variables are introduced for solving governing equations (2.2)-(2.4) as

$$\left.\begin{array}{l} u = \dfrac{v_f}{x}\sqrt{Gr}\,f'(\eta),\ v = \dfrac{v_f}{x}Gr^{\frac{1}{4}}\left\{\dfrac{\eta}{4}f'(\eta) - \dfrac{1}{2}f(\eta)\right\},\ \eta = \left(\dfrac{y}{x}\right)Gr^{\frac{1}{4}}, \\[2mm] Gr = \dfrac{x^3 g\beta_T \rho\cos(\alpha)(T_w - T_\infty)}{v^2},\ \theta = \dfrac{T - T_\infty}{T_w - T_\infty},\ \phi = \dfrac{C - C_\infty}{C_w - C_\infty}. \end{array}\right\} \tag{2.7}$$

Utilising eqn. (2.7), the fundamental eqs. (2.2) to (2.4) become

Equation of Momentum:

$$f''' + 2f' + 2ff'' - f'' - f'^2 - Mf' - \gamma(2f^2 f'' - f'^3 - ff'f'') + \theta + Nr\phi = 0. \tag{2.8}$$

Equation of Energy:

$$2\theta'' + Pr f\theta' + Pr Nb\,\theta'\phi' + Pr Nt\,\theta'^2 = 0. \tag{2.9}$$

Equation of concentration:

$$2Nb\phi'' + NbLe f\phi' + 2Nt\theta'' = 0, \tag{2.10}$$

and the governing equations that match (2.5) become

$$\left.\begin{array}{l} f = 0,\ f' = 0,\ \theta = 1,\ \phi = 1 \text{ at } \eta = 0 \\ f' \to 0,\ \theta \to 0,\ \phi \to 0 \text{ as } \eta \to \infty \end{array}\right\} \tag{2.11}$$

where involved physical parameters are defined as

$$\left.\begin{array}{l} \gamma = \gamma_1 c,\ Pr = \dfrac{\nu_f}{\alpha^*},\ M = \dfrac{\sigma B_o^2}{\rho_f c},\ Nr = \dfrac{Gr}{Re_L^2},\ Re_L = \dfrac{\Omega L^2 \sin\alpha}{\nu}, \\[2mm] Gr = \dfrac{g\beta_T \cos\alpha(T_w - T_\infty)L^3}{\nu_f^2},\ Le = \dfrac{\alpha}{D_S},\ Nb = \dfrac{\tau D_B(C_w - C_\infty)}{\nu_f}, \\[2mm] Nt = \dfrac{\tau D_T(T_w - T_\infty)}{\nu_f} \end{array}\right\} \tag{2.12}$$

The Skin-friction co-efficient is an important design parameter in thermal transit difficulties. (Cf), local Nu quantity (Nu) and Sh quantity (Sh). All such variables characterise skin-friction coefficient, heated walls, the regular including both, diffusion scores are

$$Gr^{-0.25} Nu = -\theta'(0), \tag{2.13}$$

$$Gr^{-0.25} Sh = -\phi'(0). \tag{2.14}$$

3. Numerical Solutions by R-K Method with Shooting Technique

The Runge-Kutta method, along with the shooting approach, can solve nonlinear governing equations in terms of partial derivatives. Other numerical approaches provide less precise results than this method. Using similarity transformations, the controlling partial differential equations are turned into ordinary differential equations. Using additional variables, non-linear equations are converted to linear equations. For the conversion of higher order to linear differential equations, the following additional variables are introduced.

$$f_1 = f,\ f_2 = f',\ f_3 = f'',\ f_4 = \theta,\ f_5 = \theta',\ f_6 = \phi,\ f_7 = \phi'. \tag{3.1}$$

The equations (2.8)-(2.10) are transformed to following first order ODE:

$$\left.\begin{array}{l} f_3 = f_2', \\[1mm] f_3' = -2f_2 - 2f_1 f_3 + f_3 + f_2^2 + M f_2 + \gamma(2f_1^2 f_3 - f_3^2 - f_1 f_2 f_3) - f_4 - Nr f_6, \\[1mm] f_5' = -\frac{1}{2}(Pr f_1 f_5 + Pr Nb\, f_5 f_7 + Pr Nt\, f_5^2), \\[1mm] f_7' = -\frac{1}{2}\left(Le f_1 f_7 + \frac{2Nt}{Nb} f_5'\right). \end{array}\right\} \tag{3.2}$$
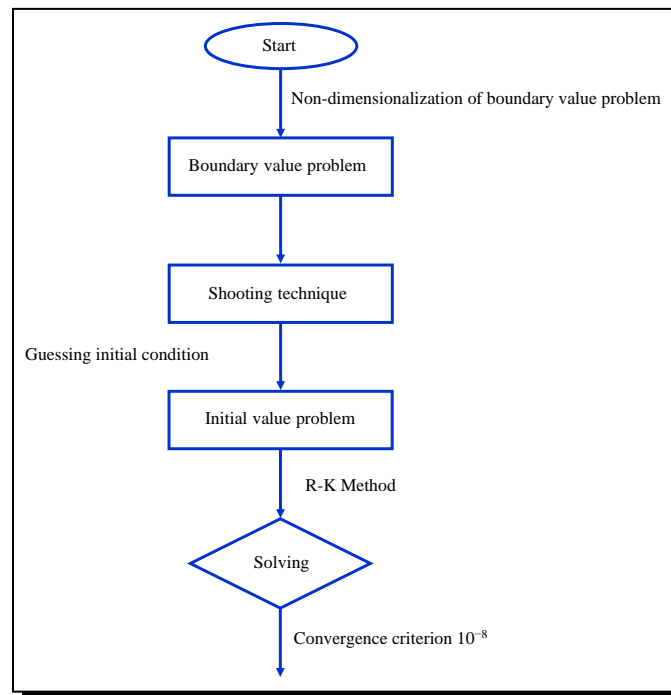
Figure 2. Flow diagram of the numerical procedure

Using eq. (3.1), the corresponding boundary conditions (2.11) are

$$\left.\begin{array}{l} f_1(0) = 0, \ f_2(0) = 0, \ f_5(0) = 1, \ f_6(0) = 1, \\ f_2(\infty) \to 0, \ f_4(\infty) \to 0, \ f_6(\infty) \to 0 \end{array}\right\} \tag{3.3}$$

To demonstrate the physical relevance of non-dimensional parameters, the approximate solutions are numerically resulting in a graphical representation using MATLAB bvp4c programming. The iterative approach is repeated until we achieve data that are accurate to a precision of 10^{-6}.

4. Program Code Validation

Table 1 demonstrates the comparison of the present numerical solutions with the pertained results in literature under some special limited cases. We found a good accuracy of the present results with the published literature. This proves the effectiveness of the obtained results and the precision of numerical technique we employed in this study.

Table 1. Comparison of present results for the Nusselt number at $M = Le = Nb = Nt = \gamma = 0$

Pr	Nr	Anilkumar and Roy [2] results	Present numerical results
1.0	0.0	0.4305	0.4264553654
	1.0	0.6127	0.6094658777
	10.0	1.0175	1.0173586909
10.0	0.0	1.4042	1.4037688432
	1.0	1.5885	1.5837690365
	10.0	2.3528	2.3476839201

5. Results and Discussion

In the present study, the free convective Maxwell-nanofluid flow moving a vertical cone in the existence of magnetic field, heat transfer, mass transfer, thermophoresis and Brownian motion effects are studied. For this study, the non-linear flow model equations are transformed into ODEs, which are evaluated analytically by applying Runge-Kutta method along with shooting method. A parametric analysis was performed, and the resulting geometric results are presented in a graphical representation to understand the problem physically. For several standards of physical parameters such as Magnetic field parameter (M), Buoyancy parameter (Nr), Maxwell fluid parameter (γ), Prandtl number (Pr), thermophoresis parameter (Nt), Brownian motion parameter (Nb) and Lewis number (Le) which are computed the velocity $f'(\eta)$, temperature $\theta(\eta)$, and species concentration $\phi(\eta)$ profiles as well as Skin-friction coefficient (Cf), Nusselt number or rate of heat transfer coefficient (Nu) and Sherwood number or rate of mass transfer coefficient (Sh) through graphs and tables. The graphical results of velocity $f'(\eta)$, temperature $\theta(\eta)$, and species concentration $\phi(\eta)$ profiles are represented in Figures 2–13 and the tabular values of Skin-friction coefficient (Cf), Nusselt number (Nu) and Sherwood number (Sh) are presented in Table 2, Table 3 and Table 4. The outcomes are calculated by assuming the values of parameters as $M = 0.3$, $Nr = 0.5$, $\gamma = 0.3$, $Pr = 0.71$, $Nt = 0.3$, $Nb = 0.5$ and $Le = 0.4$.
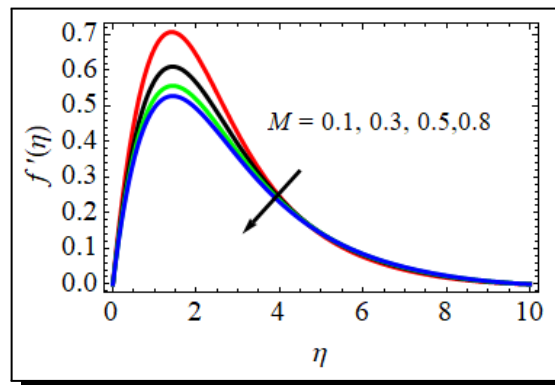

Figure 3. M influence on $f'(\eta)$ profiles
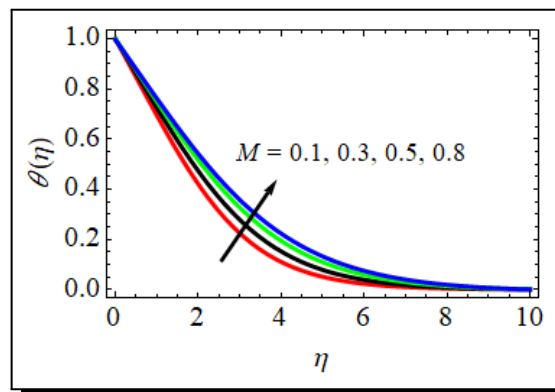

Figure 4. M influence on $\theta(\eta)$ profiles

Figures 3 and 4 illustrate the waveforms of the magnetic field parameter (M) and their effects on the temperature and flow velocity, respectively. Based on these figures, we were able to deduce that the velocity of the fluid dropped as the magnetic field rose by 0.1, 0.3, 0.5, and 0.8; in contrast, the temperature profiles revealed the behaviour of growing as the magnetic field increased. This is due to the fact that the magnetic field provides what is known as a Lorentz force, which is a decelerating body force that acts in the opposite direction of the direction of the actual magnetic field. Because of this body force, the flow of the boundary layer as well as the thickness of the momentum boundary layer are both reduced. In a similar manner, it generates heat because of the Lorentz force, which is a fractional resistive force that works against the velocity of the fluid. Because of this property, the thermal boundary layer will be greater in thickness when the magnetic field is stronger.
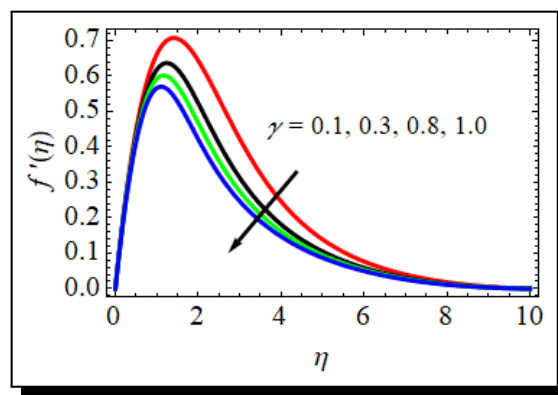

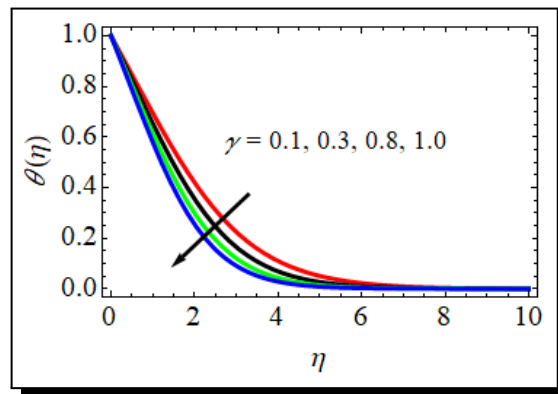**Figure 5.** γ influence on $f'(\eta)$ profiles

Figure 6. γ influence on $\theta(\eta)$ profiles

Figures 5 and 6 demonstrate the impact that the Deborah number (γ) has on the temperature and velocity curves, respectively. These figures make it abundantly evident that the thickness of the thermal boundary layer increases as the value of the Deborah number (γ) grows, but the thickness of the velocity boundary layer decreases as the value of the Deborah number rises. This is because, as the values increase, the force owing to the parameter (γ) opposes the flow of velocity and decreases thermal diffusivity in the boundary layer, which supports an increase in temperature. Additionally, as the values increase, the parameter itself has a greater influence.
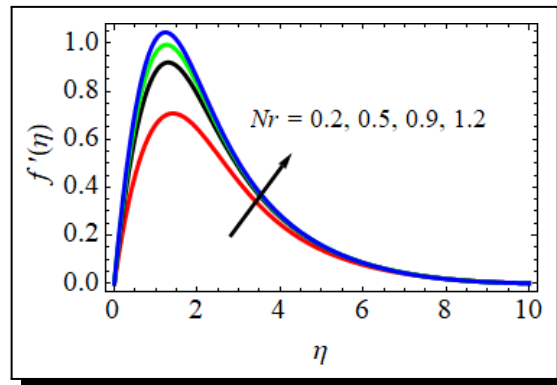
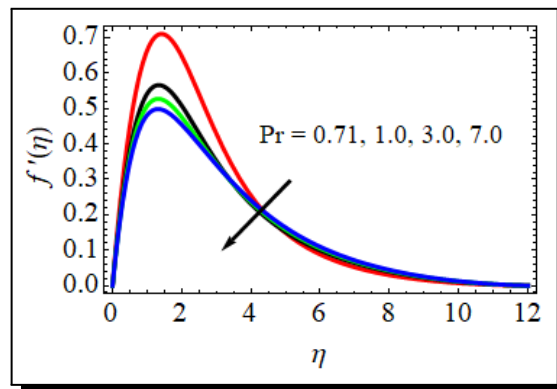**Figure 7.** *Nr* influence on $f'(\eta)$ profiles

Figure 8. *Pr* influence on $f'(\eta)$ profiles

Figure 7 depicts a plot of the influence that the buoyancy parameter, *Nr*, has on the velocity fields. It should come as no surprise that raising the buoyancy parameter would result in an increase in the velocity profiles. This is due to the fact that the buoyancy force is the driving force behind nanofluids when they are subjected to free convection. Figure 8 illustrates how varying values of the Prandtl number affect the behaviour of velocity profiles (*Pr*). According to the numerical data, the impact of higher values of the Prandtl number leads in a decreasing velocity profile. This is the case. An rise in the Prandtl number is seen to result in a reduction in the thermal boundary layer thickness and, in general, a lower average temperature inside the boundary layer. This is something that has been seen. Because higher values of *Pr* are equivalent to an increase in the thermal conductivity of the fluid, heat is able to diffuse away from the heated surface more quickly when higher values of *Pr* are present. The reason for this is that smaller values of *Pr* are equivalent to an increase in the thermal conductivity of the fluid.

Figure 9 demonstrates that the fluid temperature is decreasing, which goes against what the Prandtl number *Pr* predicts. In light of this, it may be deduced that the viscosity of the thermal boundary layer decreases as the value of *Pr* increases. This occurs for the most part due to the correlation between a high value of the Prandtl number and low thermal diffusivity, which ultimately results in a thinner thermal boundary layer. In point of fact, an increase in

the Prandtl number denotes an increase in the viscosity of the fluid, which, in turn, produces a worsening in the temperature distribution. As a result, *Pr* may be used to increase the pace at which cooling occurs in flows.
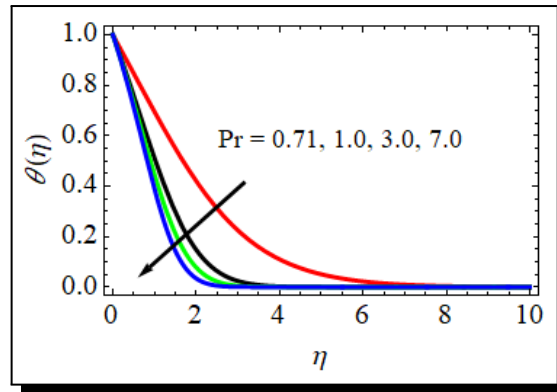

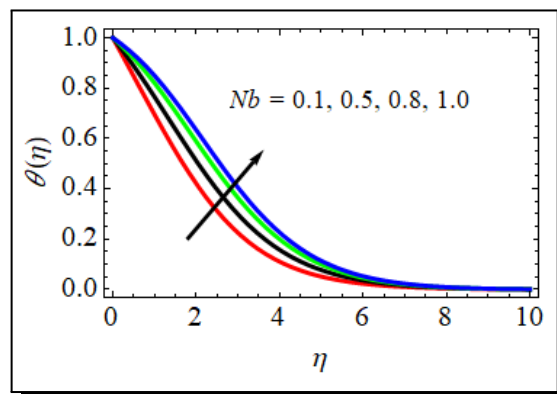**Figure 9.** *Pr* influence on $\theta(\eta)$ profiles

Figure 10. *Nb* influence on $\theta(\eta)$ profiles

The effect of Brownian motion parameter (Nb) on temperature and concentration profiles is illustrated in Figures 10 and 11 respectively. Brownian motion is the random motion of suspended nanoparticles in the base fluid and is more influenced by its fast-moving atoms or molecules in the base fluid. It is worth to mention that Brownian motion is related to the size of nanoparticles and are often in the form of cumulations and/or collections. It is noticed that, with the increasing values of Brownian motion parameter (Nb), the temperature profiles enhanced (Figure 10), whereas concentration profiles decelerate (Figure 11) in the boundary layer regime. Clearly, we noticed that the Brownian motion parameter (Nb) has significant influence on both temperature and concentration profiles. Variations of non-dimensional temperature and concentration distributions for different values of thermophoresis parameter (Nt) is depicted in Figures 12 and 13, respectively. It is noticed that both temperature and concentration profiles elevate in the boundary layer region for the higher values of thermophoresis parameter (Nt). This is from the reality that particles near the hot surface create thermophoretic force; this force enhances the temperature and concentration of the fluid in the boundary layer region.
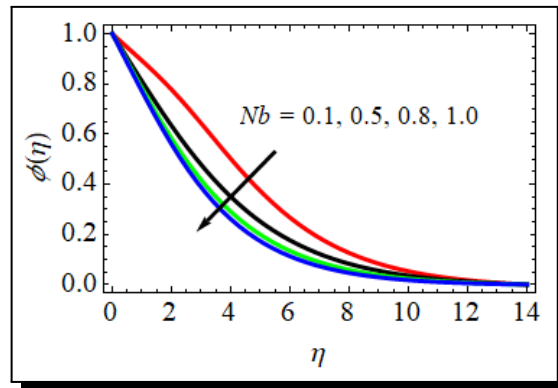
Figure 11. *Nb* influence on $\phi(\eta)$ profiles
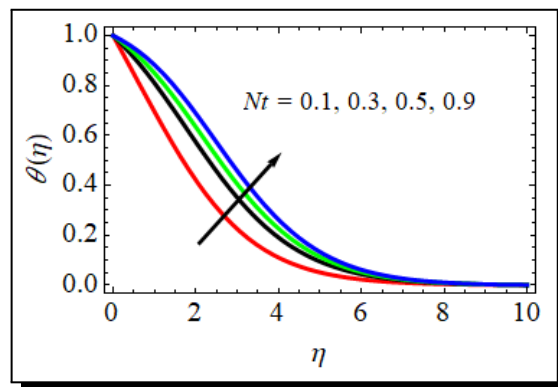
Figure 12. *Nt* influence on $\theta(\eta)$ profiles

The impact of the Lewis number (*Le*) on concentration profiles is plotted in Figure 14. It is observed that concentration distributions decelerate with the increasing values of the Lewis number in the entire boundary layer region. By definition, the Lewis number represents the ratio of the thermal diffusivity to the mass diffusivity. Increasing the Lewis number means a higher thermal diffusivity and a lower mass diffusivity, and this produces thinner concentration boundary layer.

Figure 13. *Nt* influence on $\phi(\eta)$ profiles

Table 2. Numerical values of skin-friction coefficient (Cf) for variations of M, γ, Nr, Pr, Nb, Nt and Le

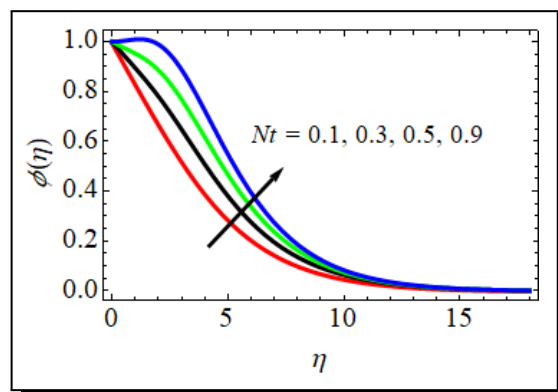| M	γ	Nr	Pr	Nb	Nt	Le	Cf
0.3	0.3	0.5	0.71	0.5	0.3	0.4	1.247756389573264
0.5							1.157883912372992
0.8							1.104674764370209
	0.8						1.214548847702334
	1.0						1.185676407200346
		0.9					1.284587287483480
		1.2					1.316743608104465
			1.0				1.175426430438059
			3.0				1.146743643280462
				0.8			1.216549830347079
				1.0			1.195673641076019
					0.5		1.275074875348085
					0.9		1.305647034786346
						0.6	1.205665934630374
						0.8	1.185603746087363

Table 2 shows the numerical values of Skin-friction coefficient (Cf) for variations in values of the engineering parameters such as, Magnetic field parameter (M), Buoyancy parameter (Nr), Maxwell fluid parameter (γ), Prandtl number (Pr), thermophoresis parameter (Nt), Brownian motion parameter (Nb) and Lewis number (Le). From this table, it is observed that the Skin-friction coefficient is increasing with rising values of Buoyancy parameter (Nr), thermophoresis parameter (Nt), Brownian motion parameter (Nb), while it is decreasing with increasing values of Magnetic field parameter (M), Maxwell fluid parameter (γ), Prandtl number (Pr) and Lewis number (Le).

Table 3. Numerical values of rate of heat transfer coefficient (Nu) for various values of Pr, Nb and Nt

Pr	Nb	Nt	Nu
0.71	0.5	0.3	0.327563976335704
1.0			0.255468731046561
3.0			0.215482165085647
	0.8		0.345638746783406
	1.0		0.367397067203693
		0.5	0.359203659705637
		0.9	0.376639706740373

Table 4. Numerical values of rate of mass transfer coefficient (Sh) for various values of Nb, Nt and Le

Nb	Nt	Le	Sh
0.5	0.3	0.4	0.256693460955639
0.8			0.215876077846743
1.0			0.186930741674316
	0.5		0.305913469392048
	0.9		0.324983741579361
		0.6	0.203307916734608
		0.8	0.176937649841641

The numerical values of rate of heat transfer coefficient in terms of Nusselt number (Nu) are displayed in Table 3 for different values of Prandtl number (Pr), Brownian motion parameter (Nb) and thermophoresis parameter (Nt). The rate of heat transfer coefficient is gradually rising with increasing values of Brownian motion parameter (Nb) and thermophoresis parameter (Nt), while the reverse effect is observed in increasing values of Prandtl number (Pr). Table 4 show the effects of Brownian motion parameter (Nb), thermophoresis parameter (Nt) and Lewis number (Le) on rate of mass transfer coefficient or in terms Sherwood number coefficient (Sh). From Table 4, it is observed that the rate of mass transfer coefficient is increasing with increasing values of thermophoresis parameter (Nt) and decreasing with increasing values of Brownian motion parameter (Nb) and Lewis number (Le).
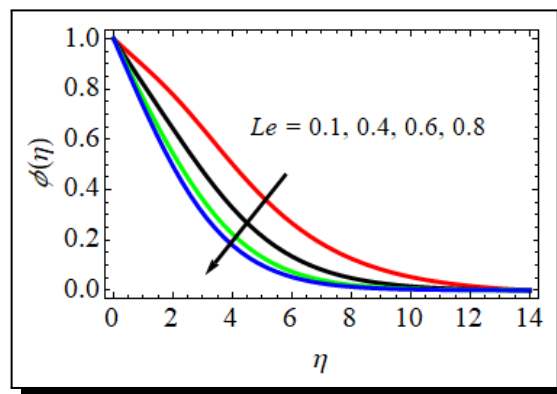
Figure 14. *Le* influence on $\phi(\eta)$ profiles

6. Conclusions

A numerical study is made for the flow of viscous, electrically conducting, incompressible, Maxwell nanofluid towards a vertical cone in the presence of magnetic field, heat transfer, mass transfer, thermophoresis and Brownian motion effects. The basic governing equations are solved by Runge-Kutta method along with shooting method. The computational procedure is revealing the nature of velocity, temperature, concentration profiles and their physical quantities due to variation of influential parameters. The salient findings are outlined as below:

- Increasing the Maxwell fluid parameter (γ) and the Magnetic field parameter (M) leads to a decline in the fluid flow.

- Buoyancy forces (Nr) are enhanced the velocity profiles.

- Rising values of Deborah number (γ), result in a decrease in temperature profiles.

- An enhancement of thermophoresis parameter (Nt) temperature and the thickness of thermal boundary layer are enhanced.

- Concentration profiles are decreases as the Brownian parameter (Nb) is decreased, whereas the thermophoresis parameter (Nt) shows the reverse trend.

- The results achieved in this work are more comprehensive form of Anilkumar and Roy [2] and can be taken as a restricting case by taking $M = Le = Nb = Nt = \gamma = 0$.

Nomenclature

List of Symbols

u, v, w	:	Velocity components in x, y and z axes respectively (m/s)
x, y, z	:	Cartesian coordinates measured along the stretching sheet (m)
f	:	Dimensionless stream function
f'	:	Fluid velocity (m/s)
C	:	Fluid concentration (mol/m^3)
B_o	:	Uniform magnetic field (Tesla)
C_∞	:	Dimensional ambient volume fraction (mol/m^3)
Nb	:	Brownian Motion parameter
T	:	Fluid temperature (K)
T_w	:	Temperature at the surface (K)
T_∞	:	Temperature of the fluid far away from the stretching sheet (K)
O	:	Origin
M	:	Magnetic field parameter
C_w	:	Dimensional concentration at the stretching surface (mol/m^3)
Cf	:	Skin-friction coefficient (s^{-1})
Pr	:	Prandtl number
Sh	:	Rate of mass transfer coefficient (or) Sherwood number
Le	:	Lewis number
Nt	:	Thermophoresis parameter
D_B	:	Brownian diffusion coefficient (m^2/s)
D_T	:	Thermophoresis diffusion coefficient (m^2/s)
c	:	Positive real number
Nu	:	Nusselt number (or) Rate of heat transfer coefficient
Gr	:	Grashof number for heat transfer
Nr	:	Buoyancy ratio parameter

g	:	Acceleration due to gravity (m/s^2)
r	:	Radius of the Cone (cm)

Greek symbols

η	:	Dimensionless similarity variable (m)
θ	:	Dimensionless temperature (K)
ρ_f	:	Density of the fluid
γ	:	Maxwell fluid parameter
ψ	:	Stream function
ϕ	:	Dimensionless fluid concentration (mol/m^3)
α^*	:	Thermal diffusivity (m^2/s)
ν_f	:	Kinematic viscosity (m^2/s)
τ	:	Ratio of nano particles heat capacity to fluid heat capacity
γ_1	:	Deborah number with respect to relaxation time
σ	:	Electrically conductivity (S/m)
β_f	:	Volumetric thermal expansion (K^{-1})

Superscript

$\prime$	:	Differentiation with respect to η

Subscripts

f	:	Fluid
w	:	Condition on the sheet
∞	:	Ambient Conditions

Competing Interests

The authors declare that they have no competing interests.

Authors' Contributions

All the authors contributed significantly in writing this article. The authors read and approved the final manuscript.

References

[1] S. Ahmad, H. H. Coban, M. N. Khan, U. Khan, Q.-H. Shi, T. Muhammad, R. Chinram and S. Kadry, Computational analysis of the unsteady 3D chemically reacting MHD flow with the properties of temperature dependent transpose suspended Maxwell nanofluid, *Case Studies in Thermal Engineering* **26** (2021), 101169, DOI: 10.1016/j.csite.2021.101169.

[2] D. Anilkumar and S. Roy, Unsteady mixed convection flow on a rotating cone in a rotating fluid, *Applied Mathematics and Computation* **155**(2) (2004), 545 − 561, DOI: 10.1016/S0096-3003(03)00799-9.

[3] R. M. Christensen, *Theory of Viscoelasticity: An Introduction*, Academic Press, London (1982), DOI: 10.1016/B978-0-12-174252-2.X5001-7.

[4] Y.-M. Chu, M. I. Khan, N. B. Khan, S. Kadry, S. U. Khan, I. Tlili and M. K. Nayak, Significance of activation energy, bio-convection and magnetohydrodynamic in flow of third grade fluid (non-Newtonian) towards stretched surface: A Buongiorno model analysis, *International Communications in Heat and Mass Transfer* **118** (2020), 104893, DOI: 10.1016/j.icheatmasstransfer.2020.104893.

[5] Y.-M. Chu, M. S. Hashmi, N. Khan, S. U. Khan, M. I. Khan, S. Kadry and Z. Abdelmalek, Thermophoretic particles deposition features in thermally developed flow of Maxwell fluid between two infinite stretched disks, *Journal of Materials Research and Technology* **9**(6) (2020), 12889 – 12898, DOI: 10.1016/j.jmrt.2020.09.011.10.1016/j.jmrt.2020.09.011

[6] Y.-M. Chu, S. Bilal and M. R. Hajizadeh, Hybrid ferrofluid along with MWCNT for augmentation of thermal behavior of fluid during natural convection in a cavity, *Mathematical Methods in the Applied Sciences* (2020), 1 – 12, DOI: 10.1002/mma.6937.

[7] V. Dumitru and R. Abdul, Stokes flows of a Maxwell fluid with wall slip condition, *Canadian Journal of Physics* **89**(10) (2011), 1061 – 1071, DOI: 10.1139/p11-099.

[8] M. R. Eid and F. Mabood, Thermal analysis of higher-order chemical reactive viscoelastic nanofluids flow in porous media via stretching surface, *Proceedings of the Institution of Mechanical Engineers, Part C: Journal of Mechanical Engineering Science* **235**(22) (2021), 6099 – 6110, DOI: 10.1177/09544062211008481.

[9] M. A. A. Hamad, Md. J. Uddin and A. I. Md. Ismail, Investigation of combined heat and mass transfer by Lie group analysis with variable diffusivity taking into account hydrodynamic slip and thermal convective boundary conditions, *International Journal of Heat and Mass Transfer* **55**(4) (2012), 1355 – 1362, DOI: 10.1016/j.ijheatmasstransfer.2011.08.043.

[10] M. Hamid, T. Zubair, M. Usman, Z. H. Khan and W. Wang, Natural convection effects on heat and mass transfer of slip flow of time-dependent Prandtl fluid, *Journal of Computational Design and Engineering* **6**(4) (2019), 584 – 592, DOI: 10.1016/j.jcde.2019.03.004.

[11] T. Hayat, S. Asghar, A. Tanveer and A. Alsaedi, Homogeneous–heterogeneous reactions in peristaltic flow of Prandtl fluid with thermal radiation, *Journal of Molecular Liquids* **240** (2017), 504 – 513, DOI: 10.1016/j.molliq.2017.05.058.

[12] D. Khan, G. Ali, A. Khan, I. Khan, Y.-M. Chu and K. S. Nisar, A new idea of fractal-fractional derivative with power law kernel for free convection heat transfer in a channel flow between two static upright parallel plates, *Computers, Materials & Continua* **65**(2) (2020), 1237 – 1251, DOI: 10.32604/cmc.2020.011492.

[13] M. N. Khan, S. Nadeem, S. Ahmad and A. Saleem, Mathematical analysis of heat and mass transfer in a Maxwell fluid, *Proceedings of the Institution of Mechanical Engineers, Part C: Journal of Mechanical Engineering Science* **235**(20) (2021), 4967 – 4976, DOI: 10.1177/0954406220976.

[14] N. M. Khan, Y.-M. Chu, M. I. Khan, S. Kadry and S. Qayyum, Modeling and dual solutions for magnetized mixed convective stagnation point flow of upper convected Maxwell fluid model with second-order velocity slip, *Mathematical Methods in the Applied Sciences* (2020), 1 – 21, DOI: 10.1002/mma.6824.

[15] M. Madhu, N. Kishan and A. J. Chamkha, Unsteady flow of a Maxwell nanofluid over a stretching surface in the presence of magnetohydrodynamic and thermal radiation effects, *Propulsion and Power Research* **6**(1) (2017), 31 – 40, DOI: 10.1016/j.jppr.2017.01.002.

[16] S. Mukhopadhyay, Heat transfer analysis of the unsteady flow of a maxwell fluid over a stretching surface in the presence of a heat source/sink, *Chinese Physics Letters* **29**(5) (2012), Article 054703, DOI: 10.1088/0256-307X/29/5/054703.

[17] A. Mythreye, J. P. Pramod and K. S. Balamurugan, Chemical reaction on unsteady MHD convective heat and mass transfer past a semi-infinite vertical permeable moving plate with heat absorption, *Procedia Engineering* **127** (2015), 613 – 620, DOI: 10.1016/j.proeng.2015.11.352.

[18] M. Nawaz, U. Arif and I. H. Qureshi, Impact of temperature dependent diffusion coefficients on heat and mass transport in viscoelastic liquid using generalized Fourier theory, *Physica Scripta* **94**(11) (2019), 115206, DOI: 10.1088/1402-4896/ab1cec.

[19] R. Rajesh and Y. R. Gowd, Heat and mass transfer analysis on MHD peristaltic Prandtl fluid model through a tapered channel with thermal radiation, *Journal of Applied and Computational Mechanics* **5**(5) (2019), 951 – 963, DOI: 10.22055/JACM.2019.27998.1450.

[20] G. K. Ramesh and B. J. Gireesha, Influence of heat source/sink on a Maxwell fluid over a stretching surface with convective boundary condition in the presence of nanoparticles, *Ain Shams Engineering Journal* **5**(3) (2014), 991 – 998, DOI: 10.1016/j.asej.2014.04.003.

[21] G. K. Ramesh, B. C. Prasannakumara, B. J. Gireesha, S. A. Shehzad and F. M. Abbasi, Three dimensional flow of Maxwell fluid with suspended nanoparticles past a bidirectional porous stretching surface with thermal radiation, *Thermal Science and Engineering Progress* **1** (2017), 6 – 14, DOI: 10.1016/j.tsep.2017.02.006.

[22] R. Ravindran, M. Ganapathirao and I. Pop, Effects of chemical reaction and heat generation/absorption on unsteady mixed convection MHD flow over a vertical cone with non-uniform slot mass transfer, *International Journal of Heat and Mass Transfer* **73** (2014), 743 – 751, DOI: 10.1016/j.ijheatmasstransfer.2014.02.053.

[23] T. Sajid, M. Sagheer, S. Hussain and M. Bilal, Darcy-Forchheimer flow of Maxwell nanofluid flow with nonlinear thermal radiation and activation energy, *AIP Advances* **8**(3) (2018), Article 035102, DOI: 10.1063/1.5019218.

[24] M. Sathyanarayana and T. R. Goud, Characteristics of MHD nanofluid flow towards a vertical cone under convective cross-diffusion effects through numerical solutions, *Heat Transfer* **52**(2) (2022), 1734 – 1753, DOI: 10.1002/htj.22761.

[25] Y.-Q. Song, H. Waqas, K. Al-Khaled, U. Farooq, S. U. Khan, M. I. Khan, Y.-M. Chu and S. Qayyum, Bioconvection analysis for Sutterby nanofluid over an axially stretched cylinder with melting heat transfer and variable thermal features: A Marangoni and solutal model, *Alexandria Engineering Journal* **60**(5) (2021), 4663 – 4675, DOI: 10.1016/j.aej.2021.03.056.

[26] J. Zhao, L. Zheng, X. Zhang and F. Liu, Convection heat and mass transfer of fractional MHD Maxwell fluid in a porous medium with Soret and Dufour effects, *International Journal of Heat and Mass Transfer* **103** (2016), 203 – 210, DOI: 10.1016/j.ijheatmasstransfer.2016.07.057.

[27] J. Zhao, L. Zheng, X. Zhang and F. Liu, Unsteady natural convection boundary layer heat transfer of fractional Maxwell viscoelastic fluid over a vertical plate, *International Journal of Heat and Mass Transfer* **97** (2016), 760 – 766, DOI: 10.1016/j.ijheatmasstransfer.2016.02.059.

[28] T.-H. Zhao, M. I. Khan and Y.-M. Chu, Artificial neural networking (ANN) analysis for heat and entropy generation in flow of non-Newtonian fluid between two rotating disks, *Mathematical Methods in the Applied Sciences* **46**(3) (2021), 3012 – 3030, DOI: 10.1002/mma.7310.

[29] T. Zhao, M. R. Khan, Y. Chu, A. Issakhov, R. Ali and S. Khan, Entropy generation approach with heat and mass transfer in magnetohydrodynamic stagnation point flow of a tangent hyperbolic nanofluid, *Applied Mathematics and Mechanics* **42** (2021), 1205 – 1218, DOI: 10.1007/s10483-021-2759-5.

[30] L. Zheng, F. Zhao and X. Zhang, Exact solutions for generalized Maxwell fluid flow due to oscillatory and constantly accelerating plate, *Nonlinear Analysis: Real World Applications* **11**(5) (2010), 3744 – 3751, DOI: 10.1016/j.nonrwa.2010.02.004.